Micron 40 (2009) 28–36

Contents lists available at ScienceDirect

Micron

journal homepage: www.elsevier.com/locate/micron

Polychromatic microdiffraction characterization of defect gradients in severely deformed materials

Rozaliya I. Barabash [a,b,*], Gene E. Ice [a], Wenjun Liu [c], Oleg M. Barabash [a]

[a] Materials Science and Technology Division of Oak Ridge National Laboratory, Oak Ridge, TN, United States
[b] Center for Materials Processing, University of Tennessee, Knoxville, TN, United States
[c] Advanced Photon Source, Argonne, IL, United States

ARTICLE INFO

Article history:
Received 7 November 2007
Received in revised form 18 February 2008
Accepted 30 March 2008

Keywords:
X-ray microdiffraction
Three-dimensional microscopy
Three-dimensional reconstruction
Severe plastic deformation

ABSTRACT

This paper analyzes local lattice rotations introduced in severely deformed polycrystalline titanium by friction stir welding. Nondestructive three-dimensional (3D) spatially resolved polychromatic X-ray microdiffraction, is used to resolve the local crystal structure of the restructured surface from neighboring local structures in the sample material. The measurements reveal strong gradients of strain and geometrically necessary dislocations near the surface and illustrate the potential of polychromatic microdiffraction for the study of deformation in complex materials systems.

© 2008 Elsevier Ltd. All rights reserved.

1. Introduction

This paper describes the use of polychromatic (white-beam) X-ray microdiffraction (PXM) to obtain three-dimensional distributions of elastic strain, lattice orientation and geometrically necessary dislocations (GNDs) near the surface of severely deformed materials. Nondestructive three-dimensional (3D) measurements of elastic strain and unpaired dislocation density distributions can now be made with an emerging class of instrumentation: the 3D X-ray crystal microscopes. These instruments use synchrotron X-ray sources and advanced X-ray optics to probe polycrystalline materials with submicron X-ray beams. By employing polychromatic X-ray beams and a virtual pinhole camera method, called differential aperture microscopy, 3D distributions of the local crystalline phase, orientation (texture) and elastic strain tensor and GNDs density tensor distributions can be measured with submicron resolution in all directions. Because the 3D X-ray crystal microscope is a penetrating nondestructive tool, it is ideal for studies of mesoscale evolution of defects near the surface of materials.

Here, we apply PXM to friction stir processed materials. Friction stir processing (FSP) is a powerful new method for joining materials and one of a growing list of processing tools that can create severely deformed and fine-grained structures at the surface of the bulk materials (Valiev, 2002; Valiev et al., 2000; Hofman and Vecchio, 2005; Zhu et al., 2004; Barabash et al., 2007). The common features for all nanostructured materials processed by FSP are high internal stresses and severe lattice distortions. Materials processed by any kind of severe plastic deformation (SPD) contain a high density of small angle boundaries and are strongly influenced by interface properties. Thus, the formation of boundaries and defect organization should be central to all investigations of these materials. At a fundamental level, insights into lattice rotations and defect organization induced by FSP improves our understanding of materials behavior during this complicated process. FSP is characterized by strong gradients of deformation and heat affected zones not present in other processes of SPD. From a practical point of view, the ability to create nanostructured regions at the surface of materials can alter their properties, and can increase their service lifetime and resistance to fatigue.

Of course X-ray diffraction characterization of materials has a long history and includes a number of techniques complimentary to PXM. With X-ray diffraction an incident beam of X-rays is efficiently reflected from a system of crystal planes when the X-ray beam satisfies Bragg's law, $2d \sin\theta = n\lambda$. Here, d is the crystal plane spacing, θ is the incident angle and λ is the X-ray wavelength. Except for a tiny refractive index correction, Bragg reflections are specular; the scattered beam and incident beams lie in the same plane and have the same angle with respect to the plane normal. In addition to the intense Bragg scattering, non-specular scattering caused by short-ranged correlations or inelastic scattering can also

* Corresponding author. Tel.: +1 865 2417230.
E-mail address: barabashr@ornl.gov (R.I. Barabash).

0968-4328/$ – see front matter © 2008 Elsevier Ltd. All rights reserved.
doi:10.1016/j.micron.2008.03.010

contribute to the overall scattering pattern and can provide information on the local correlations and/or defects. The diffuse scattering can be associated with Krivoglaz defects of the first kind (e.g. site substitution, phonons, small size objects, etc.) where the Bragg peaks remain sharp, or with Krivoglaz defects of the second kind (e.g. dislocations) where the long-range lattice rotates and the Bragg peak becomes ill defined (Krivoglaz, 1996). This diffuse scattering is most readily observed in single crystal diffraction with monochromatic parallel beam illumination. The possibility to measure lattice misorientations and geometrically necessary dislocations with monochromatic X-rays by rocking curve technique was discussed in details by (Mughrabi, 2006a,b; Wilkens et al., 1987). This approach works well for large single crystals, but sample rotations complicate the study of submicron structure in polycrystalline materials; it is difficult to keep a single submicron grain in a submicron beam during sample rotations. Such defects can also be observed in powder diffraction and/or white-beam Laue diffraction. For example, pair distribution function (PDF) analysis of short-range-structures is a rapidly evolving area of research (Egami, 1998). In standard powder diffraction technique an appropriate sample rotation (1:2) is used to achieve the optimized focusing conditions and different grains contribute to the diffraction intensity at different sample rotation angles. Strain gradients have long been observed by various glancing angle and/or energy controlled powder diffraction measurements (Hwang et al., 1988; Genzel, 1994, 1996; Zolotoyabko et al., 2004, 2006).

The PXM method described here can determine the local crystallographic orientation of small sample volumes and can nondestructively follow the evolution of individual grains or subgrain volumes (Ice and Larson, 2004; Larson and Lengeler, 2004; Larson et al., 2007; Levine et al., 2006; Liu et al., 2004; Mughrabi and Ungar, 2006; Ice and Barabash, 2007). As a characterization tool of crystal structure it has several major advantages: (1) the sample does not need to be rotated which simplifies the analysis of polycrystalline materials; (2) the intensity distributions around a large number of different reflections can be simultaneously analyzed from the same subgrain; (3) one can measure an uncompromised full three-dimensional reciprocal space intensity distribution when necessary by scanning the incident beam energy; (4) the scattering from 3D spatially resolved volumes in the sample can be measured with submicron resolution using a technique called differential aperture X-ray microscopy (DAXM) and (5) PXM together with DAXM allows the characterization of local boundary orientation and 3D interior surface morphology.

2. Polychromatic probing of crystal orientation space

2.1. Experimental setup

The basic components of the 3D X-ray crystal microscope are shown in Fig. 1a. An ultra-brilliant polychromatic X-ray beam from a type A undulator at the Advanced Photon Source (Ice and Larson, 2004; Larson et al., 2002; Larson and Lengeler, 2004; Liu et al., 2004) provides the input to the microscope. A special monochromator can be translated into the beam to transmit a narrow tunable bandpass. The polychromatic and monochromatic beams are focused at the same position and the monochromatic energy can be scanned to identify the Bragg energy of various Bragg reflections. With the monochromator out of the beam, the polychromatic X-rays pass a fixed slit and are focused onto the sample by a nondispersive total-reflection Kirkpatrick–Baez (KB) mirror pair which is used to produce a beam less than 0.5 μm $\times$ 0.5 μm. With the monochromator in the beam, a narrow-bandpass beam ($\Delta E/E \sim 1.5\,\mathrm{e}{-4}$) is deflected through the fixed slit and focused to precisely the same sample position by the KB mirror pair. As the polychromatic beam penetrates the sample, it produces a Laue pattern in each subgrain that it intercepts. The overlapping Laue patterns are detected by an X-ray sensitive CCD positioned at 90° to the incident beam. The origin of each Laue pattern can be decoded with a wire that scans through the diffracted beams (Fig. 1a).

This decoding technique is called differential aperture microscopy (DAXM). With DAXM, three-dimensional maps of the local crystallographic orientation and elastic strain tensor distributions in a sample can be constructed. The three-dimensional orientation distributions can be used to directly determine the GNDs, density tensor or Nye tensor (Nye, 1953; Larson et al., 2007). DAXM works best for polycrystalline materials with the size of grains or subgrains of the order of several microns with distinct orientation when the superposition of scattering intensities from different subgrains along the beam path is negligible.

In a typical experiment, the sample is mounted on a precision 3 axis sample stage with 25 nm bi-directional repeatability. A region of interest is identified using an optical microscope and the polychromatic X-ray beam is focused onto the sample. Overlapping Laue images from grains probed by the beam are recorded by the CCD (Fig. 1b and c). The number of grains or subgrains illuminated by the penetrating X-ray beam is identified, and the orientation of each subgrain is precisely determined by an automated indexing program. As many as 10 subgrains can be indexed simultaneously. Streaking of the Laue reflections can be used to identify the most probable GN dislocation density tensor

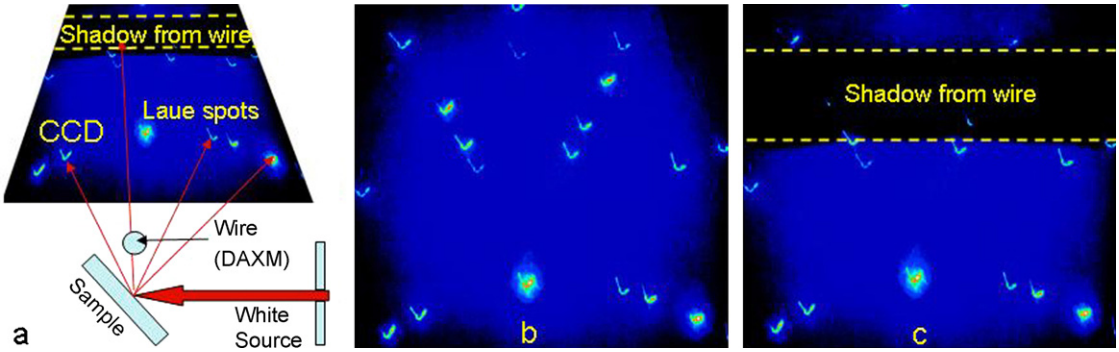

Fig. 1. (a) Schematic of the 3D X-ray crystal microscope. The polychromatic (white) X-ray source is focused onto a sample and Laue images from subgrains probed by the beam are collected by an X-ray sensitive CCD. A 50 μm wire (blue circle in the region of diffracted radiation) is used as a differential aperture (DAXM) in front of the sample to decode the depth of the radiation patterns sources. (b) Complete depth-integrated Laue pattern. (c) Partial Laue pattern with a "shadow" from the wire. Typically 400 such partial Laue patterns are taken at different positions of the wire relative to the sample surface. Together with the complete Laue pattern they are used to reconstruct the spatially resolved image coming from certain depth of the sample.

activated in the subgrain, and the number of unpaired dislocations.

2.2. Disentangling overlapping images

Because polychromatic microdiffraction produces Laue images from each subgrain intercepted by the X-ray beam, measurements are typically challenged by complex overlapping Laue patterns. The process of disentangling can be carried out either by the direct experimental use of differential aperture X-ray microscopy or by pattern matching/absorption sensitive methods (Ice and Larson, 2004; Larson et al., 2002; Larson et al., 2007; Larson and Lengeler, 2004; Liu et al., 2004). For example, the small size of X-ray beams (~500 nm) restricts the sample volume that can scatter X-rays into the CCD. The sample-volume, position is adjusted by moving the sample under the fixed X-ray beam.

The overlapping Laue patterns from the illuminated grains and subgrain volumes (Fig. 1b) are fit to find the centers of the reflections. The angles between the reflections are compared to the angles anticipated for the crystal structure of the sample. When the $n(n-1)/2$ angles between n reflections have angles that match those predicted for a particular set of reflections, the reflections are assumed to be indexed. Owing to the exquisite angular sensitivity of the measurements, once 4 or more reflections are indexed the probability for a false indexation is small. In some cases, (e.g. highly absorbing materials) the scattering volume is further limited to a near-surface region. In other cases (e.g. layered materials) the Laue patterns are distinct for different layers so the 3D position of each pattern can be inferred from the layer order.

2.3. Probing subgrain structure

For large grains and/or for single crystals scattering from different depths in the same grain complicate reconstruction of the depth-resolved images. In these cases a complementary method for characterizing the dislocation structure of small crystal volumes can be used. Here, the influence of defects on the near Bragg reflection region is modeled assuming that the probed volume is composed of single-crystal grains with defects that distort and smear the Laue reflections. This method is essential when the dislocation density is so high that the Laue spots are significantly smeared and/or streaked even from a DAXM-resolved volume, or when a significant gradient in the density distribution exists. This method complements DAXM and extends PXM analysis when:

- The length probed by the beam is small due to small grain size, thin film architecture or some other inhomogeneity/discontinuity.
- Depth probed by the beam is small in the materials with high absorption factor which complicates DAXM measurements (Ir, Pt, Ta).
- The plastic response of the material creates large strain gradient even within 1 μm and Laue spots are streaked even in the depth-resolved images obtained with DAXM (Figs. 5 and 6). Here, streak-profile analysis can be used for characterization of the GN dislocations density tensor.

An approach to characterize the dislocation structure and determine the GN dislocation density tensor by analyzing the streaked pattern by means of a multiscale hierarchical framework is described in detail in (Barabash and Ice, 2005; Ice and Barabash, 2007; Ice et al., 2005; Barabash et al., 2003).

2.4. Laue pattern streaking

In Laue diffraction, the position of every spot depends on the orientation of the diffracting volume. With a polychromatic X-ray spectrum Ewalds construction of the measurable reflections in reciprocal space is performed with Ewald spheres covering a range of radii from k_{min} to k_{min} (Fig. 2a). An energy change in the incident radiation causes a change in the Ewald sphere diameter (Fig. 2a). The micro-Laue is sensitive to radial line integrals through reciprocal space.

If the orientation changes continuously within the probed region (Fig. 2c) either due to elastic strain gradient or due to distribution of geometrically necessary (GN) dislocations, Laue spots becomes streaked (Larson et al., 2007; Barabash et al., 2003). When elastic strain gradients are small, the streaking direction is directly related to the lattice curvature and GNDs density tensor (Barabash and Ice, 2005; Ice and Barabash, 2007; Ice et al., 2005; Barabash et al., 2003). For GNDs or dislocation walls the distortion tensor, ω_{ij}, due to GN dislocations, is related to the unpaired dislocation density, n^+, and slip system (dislocation line direction τ, and Burgers vector **b**).

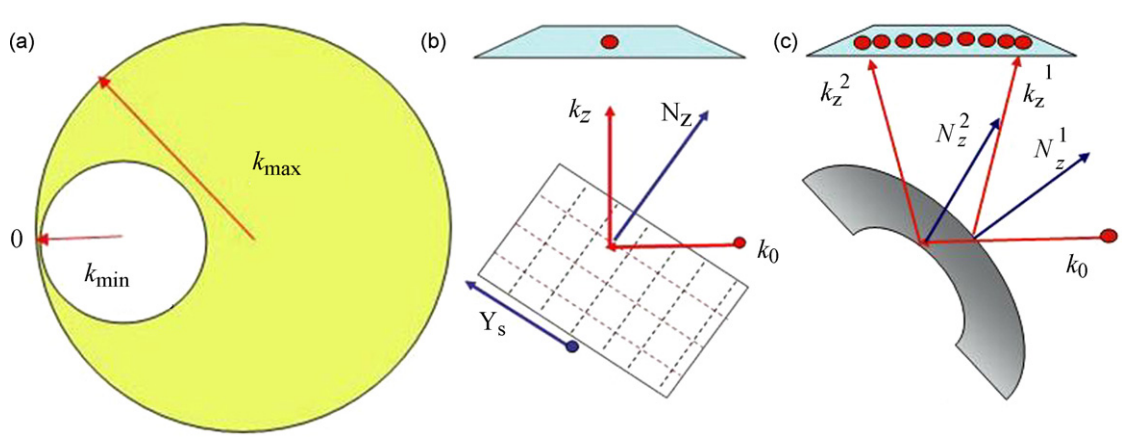

Fig. 2. (a) Polychromatic X-ray spectrum of the all reflections is performed with Ewald spheres with a range of radii from k_{min} to k_{max}. (b) Without strain gradients or GN dislocations all layers have same orientation and scatter X-rays into one spot on a CCD (red dot). (c) In crystals with strain gradients and/or GN dislocations beam probes layers with different orientation of surface normal (from $N(1/z)$ to $N(2/z)$). Different layers with distinct orientation scatter X-rays into different locations at the CCD. This results in the formation of a streak.

The length of the streak at the full width at half maximum, l, is proportional to the total number of GN dislocations and boundaries within the probed region. GN dislocations are the units of the rotational deformation modes of materials.

$$l = C_{\mathrm{Str}}\rho_{\mathrm{GN}}L \tag{1}$$

Here, C_{Str} is the contrast factor for streak; ρ_{GN} is the GN dislocation density within the probed region; and L is the length of beam path. A detailed description of the GNDs characterization with the streak analysis can be found in Barabash and Ice (2005), Ice and Barabash (2007), Ice et al. (2005), and Barabash et al. (2003).

Microfocusing optics (Ice and Larson, 2004) typically introduces a small $\leq$1 mrad* convergence to the incident beam. This convergence angle has a negligible effect along a streak, but can change the intensity distribution in the narrow direction of the streak. As a result, the experimental angular resolution function should be taken into account when using narrow streak direction to determine three-dimensional distributions of dislocations in the crystal.

2.5. Split Laue spots

If the angular misorientation through a GN boundary is sufficiently large, the orientations of the two deformation cells separated at the GN boundary become distinct, and the scattering from the above two deformation cells in incoherent. The reflection becomes discontinuous (Ice and Barabash, 2007; Barabash and Ice, 2005; Ice et al., 2005). To understand these phenomena, we assume that along the penetration depth L the X-ray beam intersects several cell blocks with average size D_{cb}. Each cell block contributes to the diffraction. The number of such contributions is L/D_{cb}. Each boundary produces an average misorientation Θ. When this misorientation exceeds the average full width at half maximum of the Laue image for each cell block along the streak direction ξ, δm_{cb}, the Laue spots split. If almost all dislocation walls are unpaired, the following criterion can be used:

$$K = \left(\frac{\Theta}{\delta m_{\mathrm{cb}}}\right) \tag{2}$$

If $K < 1$, the intensity distribution of white-beam reflection is continuous. If $K > 1$, the white-beam reflection is discontinuous, and the intensity profile along the streak consists of discrete sub-peaks.

2.6. Laue streak directions

To understand how the streaking direction is related to the distribution of GNDs within the probed region we describe the simplest case when only one edge GNDs slip system is activated. In this case the direction of the Laue streak depends on the mutual orientation of two planes:

- The plane perpendicular to the direction of GN dislocation line τ in real space.
- The plane perpendicular to the direction of reciprocal lattice vector $\mathbf{G}_{h\,k\,l}$.

The line of intersection of these two planes defines the direction of the streak axis ξ (Ice and Barabash, 2007; Barabash and Ice, 2005; Ice et al., 2005):

$$\xi = \frac{\boldsymbol{\tau} \times \boldsymbol{G}_{hkl}}{|\boldsymbol{\tau} \times \boldsymbol{G}_{hkl}|} \tag{3}$$

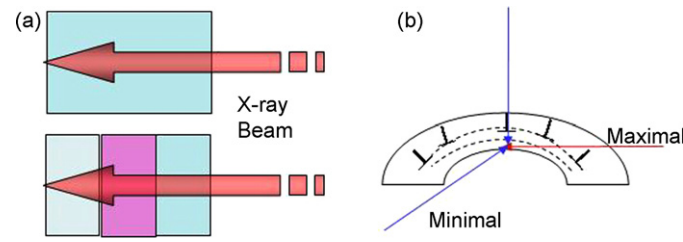

Fig. 3. (a) Sketch of the X-ray microbeam probing region of the single crystal or large grain (top), probing several grains with distinct orientations (bottom). (b) Scheme showing directions of the beam resulting in minimal (blue) and maximal (red) streaking of the Laue spot.

The second axis ν is perpendicular to the ξ axis and to the reciprocal lattice vector $\mathbf{G}_{h\,k\,l}$. With this coordinate system, the intensity of a Laue spot is elongated in the ξ direction. Directions of the beam resulting in the maximal and minimal streaking are shown in Fig. 3b.

Eq. (3) indicates that different GN dislocations slip systems should result in distinct streak orientations in the Laue patterns. Several peculiarities should be noted:

- The length of the streak (full width at half maximum in the ξ direction) δm_{ξ} depends on the orientation and the number of GN dislocations and boundaries in the probed volume.
- Along certain zone lines Laue streaks for different ($h\,k\,l$) are almost parallel to each other.
- For certain ($h\,k\,l$) no streaks are observed (or become very small). This is the case when the contrast is zero.

2.7. Lattice curvature and Nye tensor

Typically several dislocation slip systems are operating within the probed region. For example a deformation of copper single crystals with ⟨0 0 1⟩ and ⟨1 1 1⟩ load orientation involves multiple slip. When different dislocation slip systems are simultaneously activated, only components of the GN dislocation density tensor, ρ_{ij} can be unambiguously determined from the experiment.

$$\boldsymbol{\rho}_{ik} = \boldsymbol{\tau}_i \boldsymbol{b}_k \delta(r) \tag{4}$$

Here, the magnitude of the vector τ is the net number of dislocations having Burgers vector, **b**, crossing unit area normal to τ (Nye, 1953). We use the association between the elastic strain gradient tensor η_{lmk}, and lattice curvature tensor **K** with the dislocation density tensor ρ, first introduced by Kroner (1956, 1968, 1995) and further discussed in detail by Mughrabi (2006a,b, 2004), de Witt (1970), Fleck et al. (2003), Aifantis et al. (2006), Arsenlis and Parks (1999), Larson et al. (2007). The GN dislocation density tensor ρ_{ij} relates to the strain gradient tensor η_{lmk},

$$\boldsymbol{\rho} = (\mathrm{tr}\,\boldsymbol{K})\delta - \boldsymbol{K}^{*}, \text{ and in the component form } \boldsymbol{\varepsilon}_{lmk}\boldsymbol{\eta}_{lmk} = \boldsymbol{\rho}_{ik} \tag{5}$$

Here, tr **K** and **K*** are the trace and transpose of the lattice curvature tensor **K,** δ is Dirac delta function, $\varepsilon_{\tau lm}$ is the anti-symmetric Levi-Civita tensor. To analyze the dislocation sub-structure for multiple slip deformation with polychromatic microdiffraction one should first determine the lattice curvature and/or Nye tensor components from the experimental Laue pattern at each probed location. The components of the dislocation density tensor ρ_{ij} are determined unambiguously from the PXM results. Further, fitting the Laue patterns using these components allows finding the most probable GN dislocations and GN boundaries within the probed region.

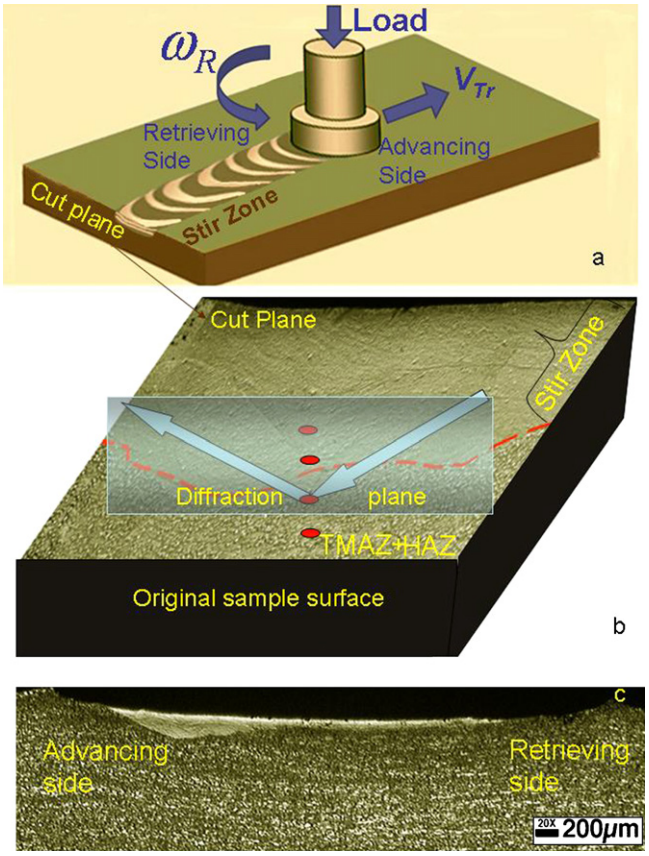

Fig. 4. (a) Sketch of the FSP tool showing the direction of transmission velocity, rotation speed and load applied to the tool. (b) Cross section of the Ti after FSP with HAZ, TMAZ and stir zones. Diffraction plane is parallel to the surface of the sample during PXM measurements. Probed locations are shown with red dots. (c) Microstructure of the FSP Ti shows asymmetry between advancing and retrieving sides.

3. Example study

Severe plastic deformation by friction stir processing is currently a subject of intense research. FSP is a very new technology that produces severe plastic deformation at the surface region of materials. This kind of deformation creates a distinct, very fine (often nanocrystalline) structure in the near-surface regions of bulk materials (Mishra and Ma, 2005; Zhu et al., 2004; Valiev, 2002; Hofman and Vecchio, 2005, 2007; Barabash et al., 2007). Physical processes in the stir zone (SZ) and in the adjacent thermo-mechanically affected and heat affected zones including strain and defects gradient distributions are largely unknown. The stirring creates heat and eventually the materials fuse and gain a new type of structure. Friction stir processing of the materials results in: (1) fast heating of the affected area to near melting temperatures; (2) severe inhomogeneous plastic deformation in the surface regions directly experiencing friction with the stir tool surface. The simultaneous influence of high temperatures and high defect density results in continuous recovery and recrystallization; the initial structure of the materials in this zone is destroyed, and new grains nucleate and grow. Here, we studied the mesoscale structures of micron, submicron and nano size grains both near the surface and under conditions which suppress recrystallization. A special tool was used for friction stir processing. The tool had an "upside down mushroom" shape without pin (Fig. 4a), rotation speed varied in the range of $\omega_R = 1.67–3.33\ s^{-1}$, transmission velocity $V_{Tr} = 0.212–0.635\ mm\ s^{-1}$, loading force $P \approx 10{,}000$ N. Simultaneous tool translation and rotation results in the movement of the material from in front of the tool to the back of the tool along a complicated trajectory.

Spatially resolved white-beam Laue X-ray microdiffraction was used to characterize the structural changes in the polycrystalline Ti. The cross section through all zones of the weld was prepared (Fig. 4b). The microbeam was running parallel to the sample surface, and at each location the diffraction plane defined by incident and diffracted beams remained parallel to the original sample surface. Probing locations were moving along lines parallel and perpendicular to the surface with a step of 2 μm. A total of 8000 locations were probed. Locations followed a 2D grid on the cut surface.

It was established that after FSP a special near-surface "so called" SZ is formed. It had a structure of a mushy zone which has been previously modeled for some other special solidification conditions (Anderson and Grae Worster, 1995; Anderson, 2003). This zone contained a mix of disordered (amorphous) and

Table 1
Typical slip systems for hexagonal crystals with Burgers vector directions—first lines and slip planes—second lines

1	2	3	4	5	6	7	8	9	10
Basal	Basal	Basal	Prismatic	Prismatic	Prismatic	Prismatic	Prismatic	Prismatic	Prismatic
$[2\bar{1}\bar{1}0](0001)$	$[\bar{1}2\bar{1}0](0001)$	$[\bar{1}\bar{1}20](0001)$	$[\bar{2}110](01\bar{1}0)$	$[\bar{2}113](01\bar{1}0)$	$[1\bar{2}13](10\bar{1}0)$	$[11\bar{2}3](1\bar{1}00)$	$[0001](1\bar{1}00)$	$[0001](10\bar{1}0)$	$[0001](01\bar{1}0)$
11	12	13	14	15	16	17	18	19	
Pyramidal	Pyramidal	Pyramidal	Pyramidal	Pyramidal	Pyramidal	Pyramidal	Pyramidal	Pyramidal	
$[\bar{1}2\bar{1}0](10\bar{1}1)$	$[2\bar{1}\bar{1}0](01\bar{1}1)$	$[\bar{1}\bar{1}20](1\bar{1}01)$	$[\bar{2}113](10\bar{1}1)$	$[1\bar{2}13](01\bar{1}1)$	$[\bar{2}113](1\bar{1}01)$	$[1\bar{2}13](\bar{1}101)$	$[11\bar{2}3](0\bar{1}11)$	$[11\bar{2}3](\bar{1}011)$	
20	21	22	23	24	25	26	27	28	
Pyramidal	Pyramidal	Pyramidal	Pyramidal	Pyramidal	Pyramidal	Pyramidal	Pyramidal	Pyramidal	
$[\bar{2}113](11\bar{2}1)$	$[\bar{2}113](1\bar{2}11)$	$[1\bar{2}13](11\bar{2}1)$	$[11\bar{2}3](1\bar{2}11)$	$[11\bar{2}3](\bar{2}111)$	$[1\bar{2}13](\bar{2}111)$	$[\bar{2}113](2112)$	$[1\bar{2}13](1212)$	$[11\bar{2}3](1122)$	

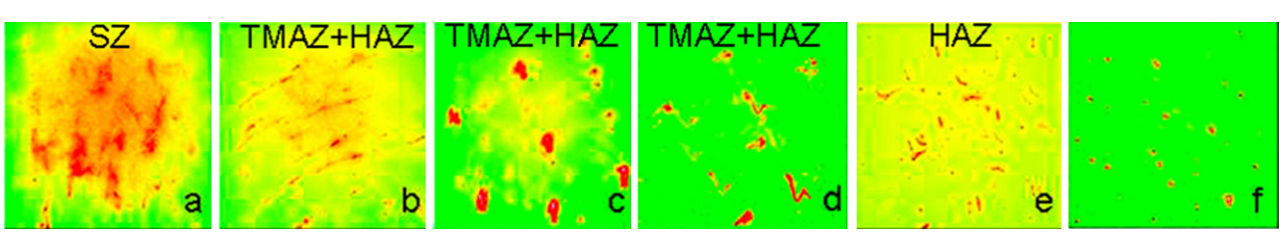

Fig. 5. Laue patterns from different zones of the polycrystalline Ti after friction stir processing. (a) Smeared Laue pattern from the mushy zone formed within the SZ; (b–e) streaked patterns from TMAZ + HAZ; and (f) base metal.

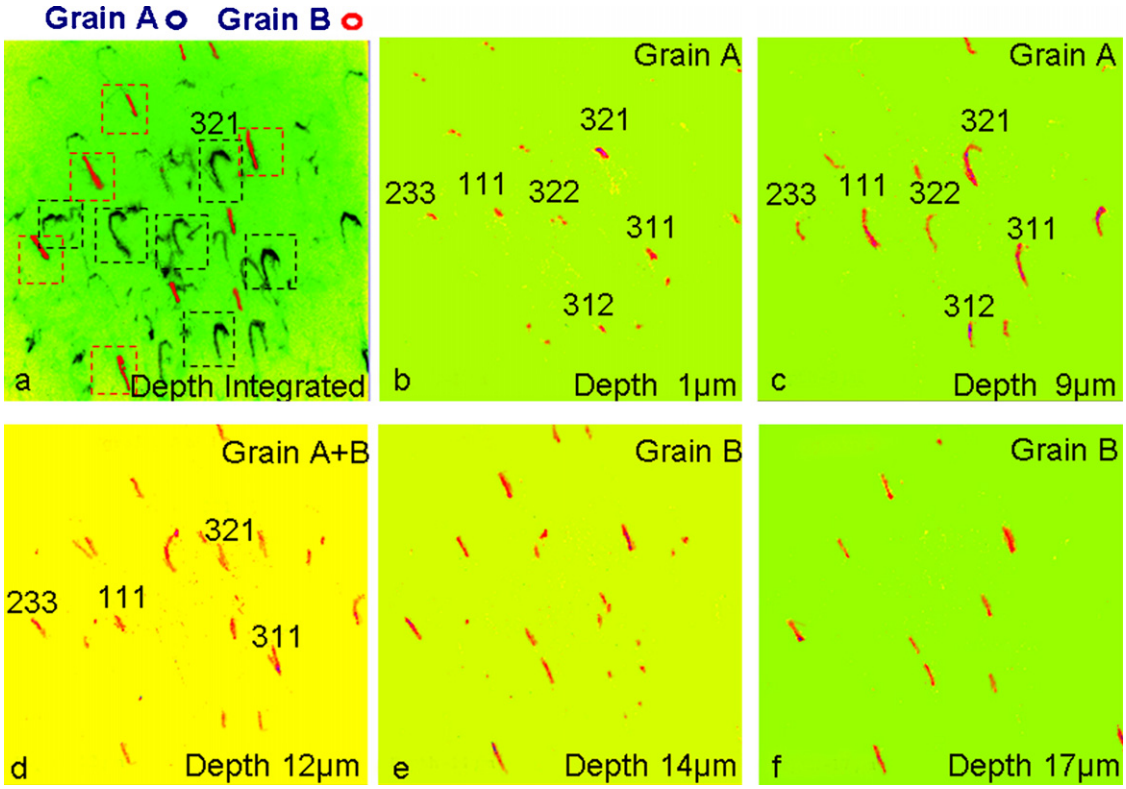

Fig. 6. Depth-integrated Laue pattern from the Ti after friction stir processing with multiples streaks (a); reconstructed Laue images at different depth under the surface (b–f). Depth in microns is shown at each frame.

nanocrystalline structures analogous to ice water. The disordered component manifests itself by a broad halo when probed with a monochromatic beam, and with a strong general background when probed with a polychromatic beam (Fig. 5a). PXM analysis of the SZ zone (with beam diameter ~0.5 μm) was extremely difficult due to complex structure of the mushy zone and strong strain gradients within the SZ: both factors smear the Laue spots (Fig. 5a). Grain size within this zone is extremely small and lies within the range of

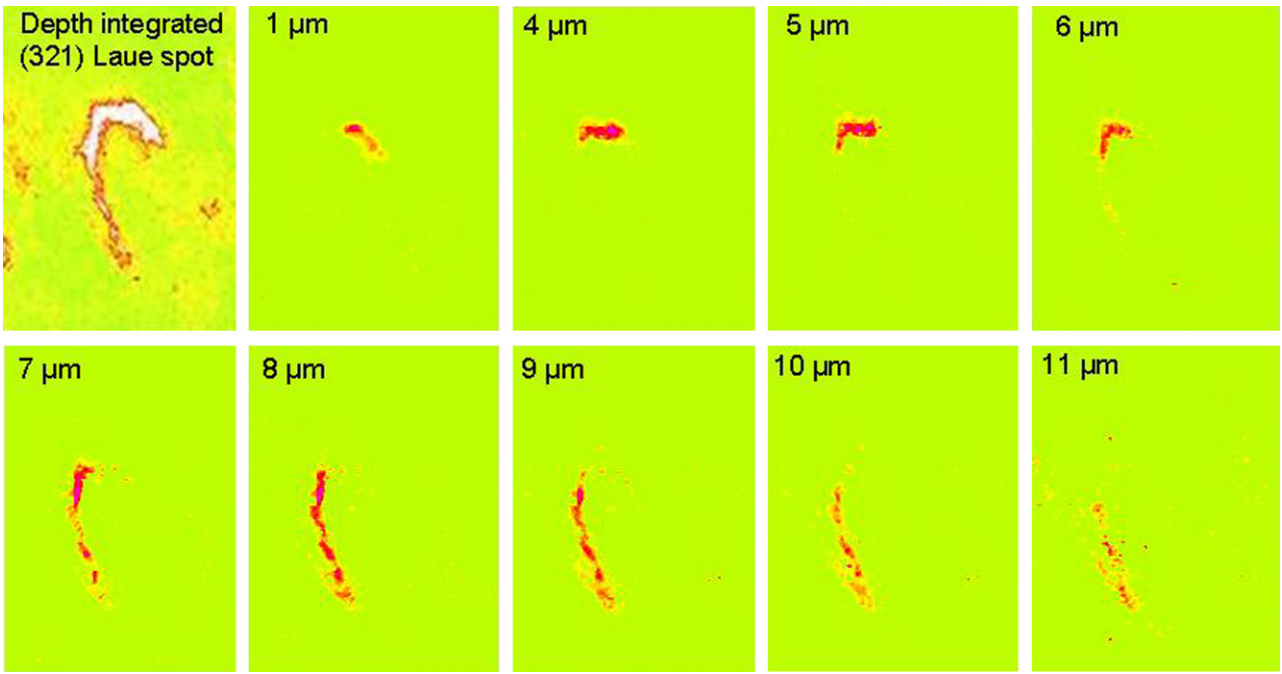

Fig. 7. Depth-integrated (3 2 1) Laue spot from grain A (left top frame) and reconstructed depth-resolved images showing intensity inputs coming from different depths of the grain A. Depth in microns is shown at each frame.

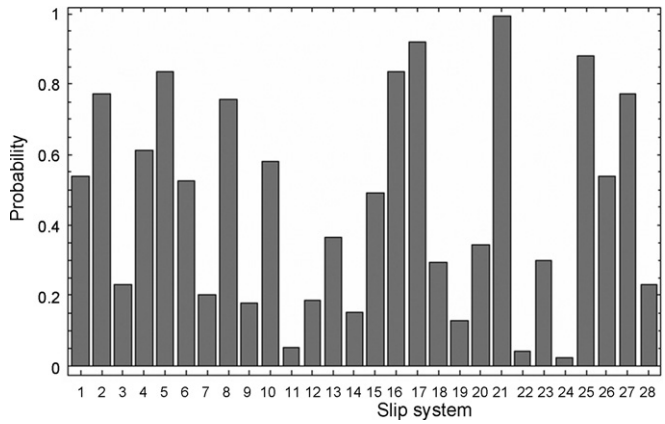

Fig. 8. Probability of different GNDs slip systems activated in grain B. Numbers along the horizontal axes correspond to slip system number in Table 1.

30–60 nm. Distinct asymmetry of the SZ was observed: the size of the zone was more than twice smaller at the advancing side as compared to retrieving side (Fig. 4c).

Underneath the nanocrystalline layer of the stir zone two additional zones are formed: a thermal mechanical affected zone (TMAZ) and a heat affected zone (HAZ). The size and structure of all zones is determined (Barabash et al., 2007). The grain size increased sharply (by two orders of magnitude) from SZ to TMAZ zones and reached several micrometers (5–30 μm) in the TMAZ. Beyond this region, the grain size decreased and reached the size typical for base material. Intensive streaking of the Laue spots is observed with a microbeam in the TMAZ and HAZ zones (Fig. 5b–e). Most of the diffraction patterns consisted of long-streaked Laue spots indicating severe plastic deformation in these zones with the formation of strain gradients, geometrically necessary dislocations and boundaries, which cause the local lattice curvature in each grain (see Section 2). Due to low absorption of X-rays in Ti, the X-ray microbeam probes layers located more then 100 μm underneath the surface. With the grain size from 5 to 30 μm in the TMAZ, several grains are typically probed by the beam.

In order to determine the most probable GNDs slip systems activated in Ti grains by FSP, the above analyzes (Section 2) was expanded for the case of GNDs in hexagonal crystals. We considered three basic kinds of GNDs Burgers vectors typical for hexagonal crystals (Klimanek and Kuzel, 1988). They correspond to Burgers vector: with zero c_0 component, $b = a_0\langle 2\,\bar{1}\,\bar{1}\,0\rangle/3$, with nonzero a_0 and c_0 components, $b = a_0\langle 1\,1\,\bar{2}\,3\rangle/3$, and with Burgers vector along the c_0 axes, $\mathbf{b} = \langle 0\,0\,0\,1\rangle$. Here, a_0 and c_0 are lattice parameters of Ti. Total of 28 slip systems were considered representing basal, prismatic and pyramidal slip (Table 1).

All probed grains along the beam path give input into the complete depth-integrated Laue pattern (Fig. 6a). Due to overlapping reflections from different grains it is impossible to index such a pattern. DAXM was applied to get spatially resolved reconstructed images from grains located at a different depth. Such images are much simpler, and it was possible to index them (Fig. 6b–f). An analysis of the depth-resolved images shows that mainly diffraction from the two grains (marked A and B) dominate the depth-integrated Laue pattern shown in Fig. 6a.

Reflections from these two grains are marked with blue (grain A) and red (grain B) rectangles. The grain A is close to surface. The boundary between grains A and B is at 12 μm (Fig. 6d). That's why reflections from both A and B grains are visible at this pattern. Strong strain gradients and lattice reorientations are observed within both grains. They result in the streaking of the Laue patterns even at the depth-resolved images corresponding to every micrometer (Fig. 6c–f).

It is worth noting that two distinct deformation modes were observed in different grains within TMAZ and HAZ. While some grains were characterized by a single rotation axes like the grain B (Fig. 6e), most of the grains demonstrated continuous change of rotation axes within the grain similar to grain A (Fig. 6c). Sometimes the direction of rotation axes changed 360° within a single grain with an average size 15–20 μm, confirming the presence of vortex deformation modes (Valiev, 2002) within these

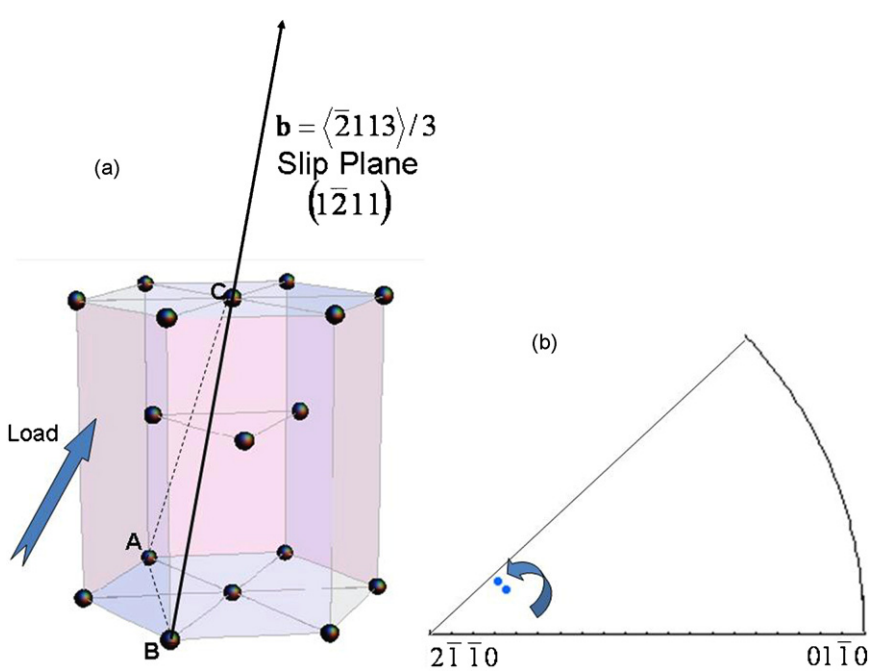

Fig. 9. (a) Orientation of FSP tool load in the hexagonal unit cell of the grain B together with most probably activated GNDs slip system. The slip plane is marked as ABC. (b) Orientation of the plastic shear strain gradient in grain B. Analysis was performed with software "Mathematica" (Wolfram, 2007).

zones. The depth dependent (3 2 1) Laue spot of the grain A is shown in Fig. 7, which illustrates continuous lattice rotations within the grain A. The (3 2 1) reflection is marked with a dashed rectangle in Fig. 6a. Analysis of the depth-resolved images complemented with streak analysis of Laue patterns indicates that grain A rotates about 5° over a depth of ~12 μm. The amount of rotation in the grain B is equal $\theta \approx 1.8°$. The surface normal of grain B is close to the $[2\,\bar{1}\,\bar{1}\,0]$ direction. The direction of the rotation axes $\boldsymbol{w}$ in grain B is close to the $[3\,1\,\bar{4}\,3]$ direction. A skew second order tensor $\boldsymbol{W}_{ij} = \boldsymbol{\varepsilon}_{ijk}\theta\boldsymbol{w}_K$, and the rotation tensor $\mathbf{R}^e$ were further determined from this rotation using the following relationship (Larson et al., 2007): $\boldsymbol{R}^e_{ij} = \cos\theta\ \delta_{ij} - \sin\theta\ \boldsymbol{\varepsilon}_{ijk}\boldsymbol{w}_K + (1-\cos\theta)\boldsymbol{w}_i\boldsymbol{w}_j$ with δ_{ij} being the Kronecker symbol. The probability of different GNDs slip systems taking part in grain B rotation is shown in Fig. 8. The most probable slip system corresponds to prismatic slip system. It has Burgers vector running in $\langle\bar{2}\,1\,1\,3\rangle$ direction and slip plane parallel to $(1\,\bar{2}\,1\,1)$ (Fig. 9a). Grain B has a favorable for slip orientation relative to the load direction (Fig. 9a), and experimentally observed lattice curvature in grain B almost exactly corresponds to plastic shear strain gradient caused by the above slip system (Fig. 9b). Assuming this slip system being activated in grain B, we determined the lower limit of GNDs density equal of $\rho_{GN} \cong 5 \times 10^9\ \mathrm{cm}^{-2}$. On the other hand, taking into account that in the simplest one-dimensional case for single slip with Burgers vector $\mathbf{b}$ in the x-direction the density of GNDs can be estimated directly from plastic shear strain gradient $\chi = \mathrm{d}\gamma^{pl}/\mathrm{d}x$ (Mughrabi, 2004) as following: $\rho_{GN} = (1/\mathbf{b})(\mathrm{d}\gamma^{pl}/\mathrm{d}x) = \chi/\mathbf{b}$, we obtain similar value of ρ_{GN}.

These results confirm that FSP induces strong lattice rotations in grains in the near-surface region of polycrystalline Ti in agreement with the model of Valiev (2002).

4. Summary

In this paper it has been shown that polychromatic microdiffraction can be used to analyze the three-dimensional mesoscale structure formed in the near-surface zone of severely deformed polycrystalline Ti after friction stir processing. Large densities of geometrically necessary dislocations and strain gradients are found in the TMAZ based on Laue microdiffraction. Dislocation density gradually decreases with depth and reaches the value typical for base material. The geometrically necessary dislocations were inhomogeneously distributed within the TMAZ and the HAZ. Inhomogeneity of geometrically necessary dislocations distribution was found at both scales: within the individual grains and between separate grains. It is established that FSP induced rotational deformation modes in Ti. This kind of deformation is realized through the nucleation and sliding of nanocrystalline grains separated with geometrically necessary boundaries. Analysis of rotational modes involves geometrically necessary dislocations and boundaries and large deviatoric strains. Such 3D spatially resolved local information about GNDs and strain gradients distribution cannot be obtained by other methods. The three-dimensional experimental technique is based on a ray-tracing algorithm of the partially shadowed with Pt wire Laue patterns. The three-dimensional reconstruction can identify the location of different grains with depth. Three-dimensional reconstructions works best for polycrystalline materials with the size of grains or subgrains of the order of several microns. Complementary streak analysis allows estimating the lattice rotations within each grain and relating it to the density of geometrically necessary dislocations. Using the above analysis the GNDs density tensor and the most probable GNDs slip systems were determined in Ti grain after FSP. The lower limit of GNDs density was estimated.

Acknowledgements

This research is supported by the Division of Materials Science and Engineering, Office of Basic Energy Science. Use of the Advanced Photon Source (W.L.) was supported by the U.S. Department of Energy, Office of Science, and Office of Basic Energy Science.

References

Aifantis, K.E., Soer, W.A., De Hosson, J.T.M., Willis, J.R., 2006. Interfaces with strain gradient plasticity: theory and experiment. Acta Mater. 54 (19), 5077–5085.
Anderson, D.M., 2003. A model for diffusion-controlled solidification of ternary alloys in mushy layers. J. Fluid Mech. 483, 165–197.
Anderson, D.M., Grae Worster, M., 1995. Weakly-nonlinear analysis of convection in a mushy layer during the solidification of binary alloys. J. Fluid Mech. 302, 307–331.
Arsenlis, A., Parks, D.M., 1999. Crystallographic aspects of geometrically-necessary and statistically stored dislocation density. Acta Mater. 47 (5), 1597–1611.
Barabash, O.M., Barabash, R.I., Ice, G.E., David, S.A., Feng, Z., Horton, J., 2007. X-ray MicroBeam characterization of the near surface nanostructured layer in Ti after friction stir processing. Rev. Adv. Mater. Sci. 15, 49–55.
Barabash, R.I., Ice, G.E., 2005. Microdiffraction analysis of hierarchical dislocation, organization. In: Encyclopedia of Materials: Science and Technology Updates, Elsevier, Oxford, pp. 1–18.
Barabash, R., Ice, G., Walker, F., 2003. Quantitative microdiffraction from deformed crystals with unpair dislocations and dislocation walls. J. Appl. Phys. 93 (3), 1457–1464.
de Witt, R., 1970. Linear theory of static disclinations. Fundamental aspects of dislocation. In: Simmons, J.A., de Witt, R., Bullough, R. (Eds.), Nat. Bur. Stand. (US), Spec. Publ. 317, I, 651–673.
Egami, T., 1998. PDF analysis applied to crystalline materials. In: Billinge, S.J.L., Thorpe, M.F. (Eds.), Local Structure from Diffraction. Plenum, New York, pp. 1–21.
Fleck, N.A., Ashby, M.F., Hutchinson, J.W., 2003. The role of geometrically necessary dislocations in giving material strengthening. Scripta Mater. 48, 179–183.
Genzel, Ch., 1996. Evaluation of stress gradients $S_{ij}(z)$ from their discrete Laplace transforms $S_{ij}(\tau_k)$ obtained by x-ray diffraction performed in the scattered vector mode. Phys. Status Solidi (a) 156, 353–363.
Genzel, Ch., 1994. Formalism for the evaluation of strongly non-linear surface stress fields by X-ray diffraction performed in the scattering vector mode. Phys. Status Solidi (a) 146, 629–637.
Hofman, D.C., Vecchio, K.S., 2005. Submerged friction stir processing (SFSP): an improved method for creating ultra-fine-grained bulk materials. Mater. Sci. Eng. A 402, 234–241.
Hofman, D.C., Vecchio, K.S., 2007. Thermal history of friction stir processes and submerged friction stir processed aluminium. Mater. Sci. Eng. A 465, 165–175.
Hwang, B.B., Houska, C.R., Ice, G.E., Habenschuss, A., 1988. Residual strain gradients in a fully stabilized zirconia sample. J. Appl. Phys. 63, 5351.
Ice, G.E., Larson, B.C., 2004. Three dimensional X-ray structural microscopy using polychromatic microbeams. MRS Bull. 29 (3), 170–176.
Ice, G., Barabash, R., Pang, J., 2005. Polychromatic X-ray microdiffraction characterization of local crystallographic structure and defect distribution. In: Encyclopedia of Materials: Science and Technology Updates, Elsevier, Oxford.
Ice, G.E., Barabash, R.I., 2007. White beam MicroDiffraction and dislocations gradients, in series. Dislocations in Solids 13, 500–601 (Chapter 79).
Klimanek, P., Kuzel, R., 1988. X-ray diffraction line broadening due to dislocations in non-cubic materials. I. General consideration and the case of elastic isotropy applied to hexagonal crystals. J. Appl. Cryst. 21, 59–66.
Krivoglaz, M.A., 1996. X-ray and neutron diffraction. In: Moss, S.C., Peisl, J. (Eds.), Nonideal crystals. Springer, New York, p. 466.
Kroner, E., 1956. Z. Naturforsch. 11a, 969.
Kroner, E., 1968. Mechanics of generalized continua. In: Kroner, E. (Ed.), Proc. IUTAM Symposium, Freudenstadt-Stuttgart, 1967. Springer-Verlag, Berlin, p. 200.
Kroner, E., 1995. Dislocations in crystals and in continua: a confrontation. Int. J. Eng. Sci. 33 (15), 2127–2135.
Larson, B.C., Wenge Yang, Ice, G.E., Budai, J.D., Tischler, J.Z., 2002. Three dimensional X-ray structural microscopy with sibmicrometer resolution. Nature 415 (21), 887–890.
Larson, B.C., El-Azab, A., Yang, W.G., Tischler, J.Z., Liu, W.J., Ice, G.E., 2007. Experimental characterization of the mesoscale dislocation density tensor. Philos. Mag. 87, 1327–1347.
Larson, B.C., Lengeler, B., 2004. High-resolution three dimensional microscopy. MRS Bull. 29 (3), 152–154.
Levine, L.E., Larson, B.C., Yang, W., Kassner, M.E., Tischler, J.Z., Delos-Reyes, M.A., Fields, R.J., Liu, W., 2006. X-ray microbeam measurements of individual dislocation cell elastic strains in deformed single-crystal copper. Nat. Mater. 5, 619–622 (Letters).
Liu, W., Ice, G.E., Larson, B.C., Yang, W., Tischler, J.Z., Budai, J., 2004. The three dimentional X-ray crystal microscope: a new tool for materials characterization. Metall. Mater. Trans. A 35A, 1963–1967.

Mishra, R.S., Ma, Z.Y., 2005. Friction stir welding and processing. Mater. Sci. Eng. R 50, 1–78.
Mughrabi, H., 2006a. Dual role of deformation-induced geometrically necessary dislocations with respect to lattice plane misorientations and/or long-range internal stresses. Acta Mater. 54, 3417–3427.
Mughrabi, H., 2006b. Deformation-induced long-range internal stresses and lattice plane misorientations and the role of geometrically necessary dislocations. Philos. Mag. 86, 4037–4054.
Mughrabi, H., 2004. On the current understanding of strain gradient plasticity. Mater. Sci. Eng. A 387–389, 209–213.
Mughrabi, H., Ungar, T., 2006. Close up on crystal plasticity. Nat. Mater. 5, 601–602 (Letters).
Nye, J.F., 1953. Some geometrical relations in dislocated crystals. Acta Metall. 1, 153–162.
Valiev, R., 2002. Nanomaterial advantage. Nature 419, 887–889 (Letters).
Valiev, R., Islamgaliev, R.K., Alexandrov, I.V., 2000. Bulk nanostructured materials from severe plastic deformation. Prog. Mater. Sci. 45, 103–189.
Wilkens, M., Ungar, T., Mughrabi, H., 1987. X-ray rocking-curve broadening of tensile-deformed (0 0 1)-oriented copper single crystals. Phys. Status Solidi (a) 104, 157–170.
Wolfram, S., 2007. Mathematica, Ver.6.0, Wolfram Media.
Zhu, K.Y., Vassel, A., Brisset, F., Lu, K., Lu, J., 2004. Nanostructure formation mechanism of α-titanium using SMAT. Acta Mater. 52, 4101–4110.
Zolotoyabko, E., Pokroy, B., Quintana, J.P., 2004. Depth-resolved strain measurements in polycrystalline materials by energy- variable X-ray diffraction. J. Synchrotron Radiat. 11, 309–313.
Zolotoyabko, E., Pokroy, B., Cohen-Nyams, T., Quintana, J.P., 2006. Depth-resolved strain measurements in thin films by energy-variable X-ray diffraction. Nucl. Instrum. Methods Phys. Res. B246, 244–248.